Engineering Geology 341 (2024) 107701

Contents lists available at ScienceDirect

Engineering Geology

journal homepage: www.elsevier.com/locate/enggeo

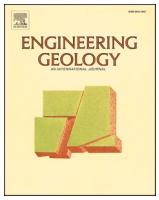

Mapping 1D seismic amplification effects in the range of periods of engineering interest based on geological data

P. Pieruccini [a], P.L. Fantozzi [b], N. Carfagna [b], I. Gaudiosi [c], D. Albarello [b,c,*]

[a] Department of Eart Science, University of Turin, Turin, Italy
[b] Department of Physical Science, Earth and Environment, University of Siena, Siena, Italy
[c] Consiglio Nazionale delle Ricerche, Istituto di Geologia Ambientale e Geoingegneria, Montelibretti, Italy

ARTICLE INFO

Keywords:
Site response
Seismic microzonation
Seismic hazard
Geological maps
Numerical simulations
Equivalent linear approach

ABSTRACT

Regional scale seismic hazard assessment including the effect of local seismo-stratigraphical conditions is a basic tool for seismic risk estimates. A novel physically based procedure is proposed for using geological maps to extensively estimate expected seismic amplification effects relative to spectral ordinates of main engineering interest (<0.8 s). Automatic GIS based analysis of geological maps, statistical data relative to the seismic/geotechnical properties of geological units and numerical modelling are combined to determine the probability distribution of expected amplification effects by accounting for uncertainty affecting the relevant parameters. To evaluate the feasibility of the proposed procedure, it has been applied to the Tuscany Region in Central Italy. Unbiasedness of outcomes has been tested by considering detailed microzonation studies available for the considered area. Results of the proposed approach could be easily implemented in extensive seismic risk analyses where detailed seismic microzonation studies are lacking.

1. Introduction

Emergency planning, development of effective land and city management aiming at reducing the of future earthquakes, seismic risk evaluations relative to distributed networks (lifelines, etc.) and other assets of economic interest exposed to earthquakes require a large scale assessment of seismic hazard. In most countries, a seismic hazard map at national scale is available only for a reference subsoil configuration. As concerns Italy, a seismic hazard model has been provided (Stucchi et al., 2011) and a uniform probability response spectrum has been made available relative to each site of the country (http://esse1.mi.ingv.it/) relative to an 'engineering bedrock' characterized flat morphology and shear wave velocities larger than 800 m/s (CEN, 2004). However, to be applied for practical purposes (e.g., seismic risk estimates), spectral ordinates provided by the hazard model must be modified to account for the local morpho-stratigraphical conditions (e.g. Kramer, 1996). In principle, this requires site specific studies relative at the scale of tens to hundreds of meters and substantial investment in geological and geotechnical data acquisition as well as interpretation, which cannot be affordable at regional scale. This is why several attempts have been performed around the World (Wald and Allen, 2007; Allen and Wald, 2009; Thompson and Wald, 2012; Thompson et al., 2014; Kwok et al., 2018; Vilanova et al., 2018; Pontrelli et al., 2023) to provide large scale estimates of site effects to allow a first glance application of hazard maps when detailed studies are lacking. These studies aim at taking advantage of information widely available at national scale, such as digital terrain models and geological maps. In general, the basic tool is the definition of a statistical correlation between any morphometric index and/or or geological outcrop and a synthetic parameter (Vs30 corresponding to the harmonic average of Vs values down to 30 m of depth) assumed to be representative of the local seismic response. As concerns Italy, a similar approach based on geological data has been firstly proposed Di Capua et al. (2016) and refined by Forte et al. (2019) based on a geological map of Italy at the scale 1:100.000. More recently, Mori et al. (2020a), Falcone et al. (2021) and Mendicelli et al. (2022) proposed a more advanced approach based on the joint application of a statistical analysis of morphometric data (available at the scale of ten meters) and numerical simulations to provide a new Vs30 map of Italy and relative uncertainty. The aim of the present study is providing a new methodology to estimate of 1D amplification effects at regional scale in Italy by using as a proxy of data from detailed geological maps (at the scale 1:10.000). The main methodological novelty of the proposed approach is the use of an automatic GIS based approach to reconstruct from available geological maps the stratigraphic succession at each outcrop.

* Corresponding author at: Department of Physical Science, Earth and Environment, University of Siena, Siena, Italy.
E-mail address: dario.albarello@unisi.it (D. Albarello).

https://doi.org/10.1016/j.enggeo.2024.107701
Received 27 May 2024; Received in revised form 21 August 2024; Accepted 26 August 2024
Available online 30 August 2024

This information is combined with numerical simulations to obtain a probabilistic estimate of expected amplification effects. This combination of distributed information and numerical analyses is similar to the one adopted to hazard estimates relative to earthquake induced landslides (Jin et al., 2024; Ojomo et al., 2024).

Since the procedure here proposed aims at providing extensive estimates of amplification effects to be used for emergency and land planning at the scale of a municipality and providing large scale risk estimates, outcomes are expressed in terms of synthetic amplification factors (AF in the following) defined as

$$AF_{T_1,T_2} = \frac{\int_{T_1}^{T_2} Sa_o \, dT}{\int_{T_1}^{T_2} Sa_b \, dT} \quad (1)$$

where Sa_o and Sa_b respectively represent spectral ordinates of the estimated response spectrum as function of the natural period T of buildings (assuming a 5 % of damping) at the outcrop and at the outcropping engineering bedrock; the upper and lower integration limits (T_1 and T_2) respectively identify short (0.1–0.5 s), intermediate (0.4–0.8 s) and long period (0.7–1.1 s) ranges. This parametrization has been adopted by the Italian Guidelines for Seismic Microzonation (SM Working Group, 2015) to optimize the application of microzonation outcomes for emergency and land planning, and seismic risk assessment (Mori et al., 2020b).

The details of the approach here proposed are presented at first. Then its application to the Tuscany Region (Central Italy, covering about 23,000 km^2) is presented and tested tested by considering estimates provided by detailed seismic microzonation studies available in the study area (Albarello, 2017; Moscatelli et al., 2020).

2. Overview of the procedure

Step 1: Morpho stratigraphic and lithological re-classification of geological outcrops.

A key element of the proposed procedure is the analysis of available geological maps where outcropping geological formations are classified according to lithostratigraphic criteria. Information provided in the maps (e.g. formation, lithology, thickness, bedding, geological boundary, excavations, faults and fractures, engineering geological classification, soil testing, geophysical testing, etc.) are stored in the spatial database. By following Pieruccini et al. (2022) outcrops are firstly classified as “Coverage” or ‘Geological Bedrock” terrains. The cover terrains are mainly associated with loose Quaternary deposits affected by recent dynamics of local geomorphological factors and are cartographically identifiable in specific morphological contexts (valley and slope, slope, etc.)). The bedrock terrains belong to the Pliocene and pre-Pliocene terrains.

Thus. Morpho Stratigraphic Domains for the study area (‘MSD’ in the following) are identified based on the stratigraphical setting (i.e. vertical order and relationships, dominant lithology), the tectonic style (i.e. basins and ridges) and geomorphology (i.e. overall morphometry and associated surface processes) by following Cesarano et al. (2022) and Pieruccini et al. (2022). Each unit belonging to the considered MSD is related to the units of the other MSDs by their reciprocal stratigraphical positions (i.e. over- or underlying). Based on the geological map, a range of possible thickness value and the prevailing lithotype (Table 1) are associated to each outcrop of the considered MSD.

Step 2: reconstructing seismo-stratigraphic succession at each outcrop.

A semi-automatic GIS bases spatial analysis is then performed to infer the stratigraphic setting (local Log) of each outcrop, based on the geological map by accounting for the stratigraphic relationships defined as described above. To this purpose, surrounding outcrops within a radius of 500 m from the boundaries of the outcrop of concern, are considered. This value is obtained by assuming an average dip of the contacts between the overlapping morpho stratigraphic MSDs by 30° and the need to reach a maximum depth of 300 m below the outcrop surface. The respective stratigraphic order of these surrounding outcrops is then considered to assess the possible stratigraphic configuration in the assumption that the Log may include three overlapping MSDs as a maximum. An example is shown in Fig. 1 to illustrate how the Arcpy™ script was created in the ArcGIS Pro™ platform to perform this analysis.

Table 1
Simplified lithotype classification groups adopted in the present study as proposed by Romagnoli et al. (2022) and Gaudiosi et al. (2023).

Cover terrains	
G	Terrains containing remains of human activity, anthropogenic deposits; well sorted and not sorted gravels, mixed gravels and sands; silty and clayey gravels, mixed gravels, sands silts and clays
S	Well and not sorted sands, mixed sands and gravels; silty and clayey sands, mixed sands, silts and clays; Inorganic silts, fine sands, diatomic silts; Inorganic silts, fine silty-clayey sands, low plasticity clayey, silts
C	Organic silts, low plasticity organic silty-clays; middle and middle-low plasticity organic and inorganic clays, organic silts, gravel-sandy clays, silty clays; high plasticity inorganic clays; peat and organic soils
Geological bedrock	
L	Non stratified and stratified lapideous rock including fractured and weathered
V	Stratified and not stratified grainy cemented rock, stratified, and not stratified alternations of lithotypes, cohesive over-consolidated rock
W	Stratified cohesive over-consolidated rock, fractured/weathered both stratified and not stratified grainy cemented rock, fractured/weathered alternations of lithotypes, fractured/weathered cohesive over-consolidated rock

The outcropping areas of the different MSDs are registered in the spatial database as “georeferenced polygonal layers” having reference planimetric cartographic coordinates, which therefore allow the analysis of the different spatial relationships between the polygons representing the areas, using common spatial criteria analysis techniques available in GIS Platforms. As shown in Fig. 1A, each polygonal area belonging to each MSD is classified in terms of the relative stratigraphic position in line with the classification developed in the first step of the analysis. In the example in Fig. 1, each outcrop is identified by a number (increasing from the one stratigraphically shallower to the deeper one) and a letter representative of the prevailing lithotype class (Table 1) for each outcrop in the considered area. In the example in Fig. 1, the target is reconstructing the stratigraphy relative to the MSD 11 (panel B in Fig. 1). Then a 500 m wide buffer area around the single selected area is built (Panel C in Fig. 1) and all polygons intersecting the buffer are considered as a possible member of the stratigraphic Log. All the other outcrops relative to deeper MSDs are then considered up to three layers at maximum. Based on the stacking order, the polygons of the other underlying MSD (MSDs 12, 30 and 41 in this example) are selected (see Table 2) by considering the prevailing lithology at each outcrop. The MSD and lithotype of the selected polygons (identified in the Frame D of Fig. 1 by underlined labels), are processed for their extraction, sorted according to the stacking order and grouped based on their unique value by considering prevailing lithologies at each outcrop. In this example, the Logs are composed of the upper horizon composed of three units (MSD 11 with lithotype G; MSD 12 with lithotype S; MSD 12 with lithotype G) superimposed on the lower horizon composed of MSD 30 with lithotype V superimposed again on the lower horizon MSD 41 with lithotype V. In this way, the Log relative to the considered polygon is built by considering the thickness ranges assessed for the considered MSDs in the first step on the analysis. The deeper layer (MSD 41) is excluded because it exceeds the maximum number of allowed layers in the Log.

In each new selection step of spatial analysis for the different MSDs’ group of units, the procedure excludes the MSDs already been processed from the analysis: in practice, the analysis proceeds from the upper to

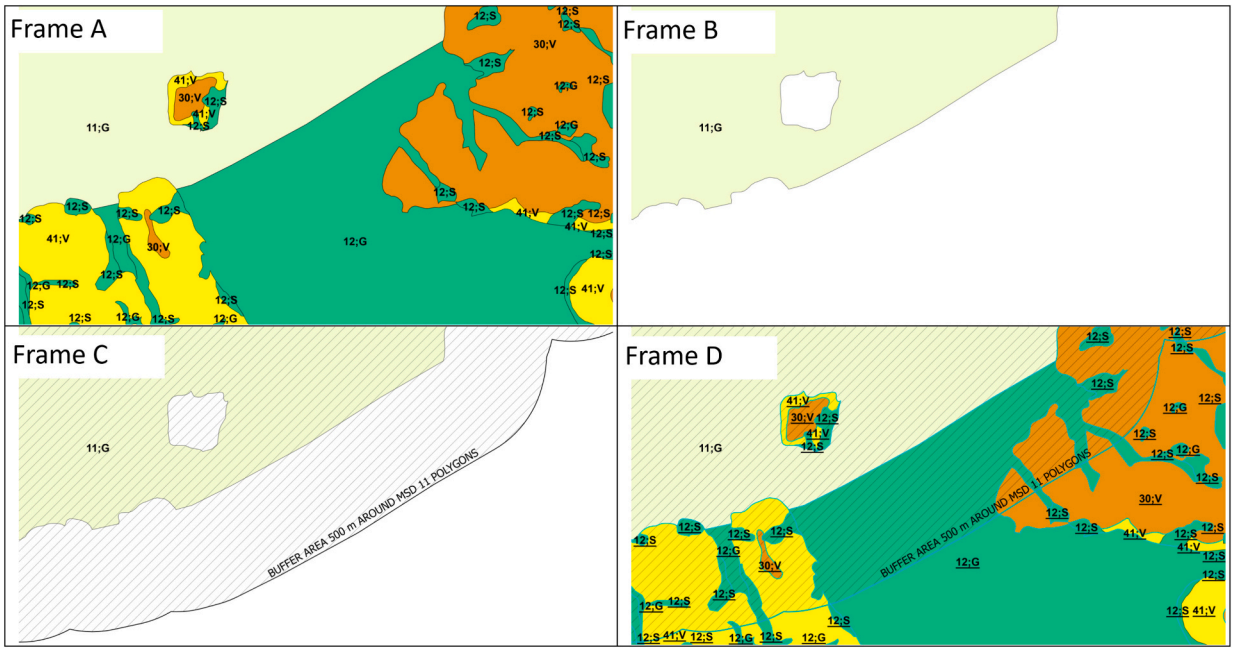

Fig. 1. Example relative to the procedure adopted to reconstruct the stratigraphic log relative to a single outcrop. The first step consists in selecting any outcrops from the MSDs map (Frame A) belonging to the upper litho-morpho-tectonics and creating a temporary layer (MSD 11 in Frame B). The third step creates a 500 m wide buffer area around any temporary layer polygon and selects all other outcrops within this buffer area (Frame C). The MSD and lithotype for the selected polygons are in the frame D with underlined labels.

Table 2
Table summarizing the actual Log obtained by the automatic procedure relative to the case in Fig. 1. Letters indicate the prevailing lithology (Table 1) relative to the considered MSDs. Colours correspond to the ones in Fig. 1.

MSD	Lithologies	Thickness range	
11	G	50-100	Cover Terrain
12	C, G, S	3-50	Cover Terrain
30	V	3-50	Geologic Bedrock
41	V	3-300	Geologic Bedrock

the lower units.

Step 3: numerical modelling.

Numerical modelling is considered to estimate 1D seismic amplification effect relative to each outcrop of the considered MSDs. The succession of units relative to each outcrop determined as above is parameterized in terms of geometrical, mechanical, and seismic properties relevant for modelling seismic amplification phenomena in the linear equivalent approach (Schnabel et al., 1972). In particular, based on the lithotype associated to the considered outcrop, the shear wave velocity (Vs) profile as a function of depth and the respective range of variability are determined on the basis of the statistical analyses by Romagnoli et al. (2022). As concerns, information concening non linear dynamical soil properties (G/G0 and damping curves along the respective range of variability) have been determined by Gaudiosi et al. (2023) and refined in the present study (see the Appendix). To account for the statistical variability of the relevant parameters and evaluating its effect on the expected amplification values, several random profiles is defined for each considered outcrop. The randomization procedure is performed as follows:

a) For each layer in the sequence, a thickness value is randomly extracted by a uniform distribution defined in the range of possible values defined at the Step 1 on the basis of the geological model; in the case that the lithotype of that layer is uncertain, is attributed randomly by choosing one of the possible alternatives as defined in the Step 2 for that layer; in this way, a single sequence of layers is built for the considered outcrop;
b) The sequence is then discretized as stack of thin layers each thick 1 m; depending on the gt-group and depth, a Vs value is defined for each sub-layer by randomly extracting values from the log-normal probability distributions defined by Romagnoli et al. (2022), also accounting for possible correlation between Vs value relative to subsequent layers. The depth of the engineering bedrock where the input motion is applied, is defined for each simulated profile as corresponding to the depth below which all Vs values exceed 800 m/s. In the same way, to each sublayer G/G0 reduction and damping curves are randomly attributed as a function of the lithotype and depth by following Gaudiosi et al. (2023). Details relative to the proposed parameterization are provided in the Appendix.
c) By considering the Inverse Random Vibration Theory (Rathje and Ozbey, 2006) and the equivalent linear numerical modelling, the expected seismic response is determined for each possible seismostratigraphical profile obtained for that outcrop (see Falcone et al., 2021 for details). In the considered simulation, input motion has been applied where Vs values overcome 800 m/s, which is the definition of engineering bedrock considered in the Italian seismic code.

The procedure described above has been implemented in the numerical code NC92Soil (Acunzo et al., 2024) and iterated 100 times for each outcrop to obtain representative values for the parameters of interest. In the assumption that Amplification Factors in eq. [1] can be considered as log-normal random variates, median and the standard deviation of AF values (in logarithm) resulting from the simulations will be considered as representative of the population of the possible values for the outcrop of concern. An example of outcomes from the procedure described above relative to a single outcrop is shown in Fig. 2.

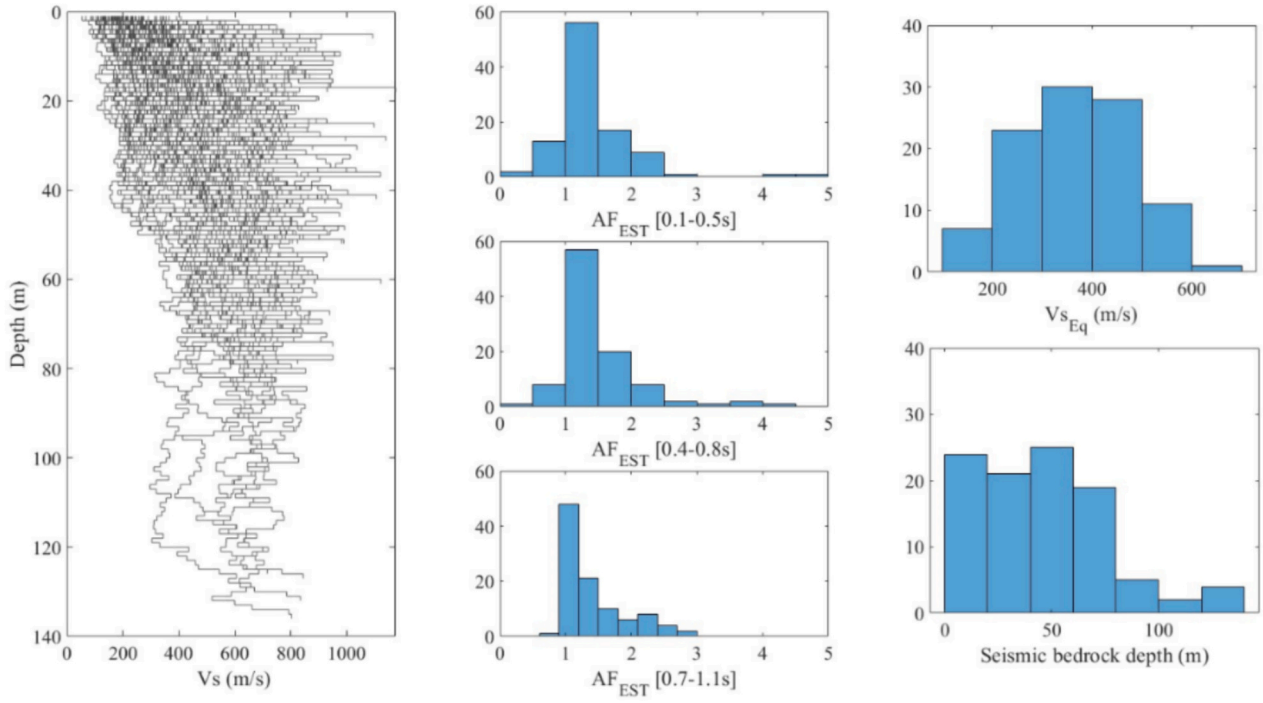

Fig. 2. Outcomes of the numerical simulations relative to a single outcrop. 100 profiles were randomly generated accounting for available constraints (plot in the left). Distribution of AF values estimated by numerical simulations in the three ranges of periods (AF_{EST}) are reported in the three histograms in the center of the figure. The two histograms in the right respectively report the frequency distribution of Vs_{eq} values (the harmonic average of Vs values down to 30 m from the surface or to the depth of the engineering bedrock when it is lower than 30) and of the depths of the engineering bedrock considered in the simulations.

3. Application to the Tuscany region

The Tuscany region is in the central western side of the Italian peninsula and it is characterized by a complex territory, with heights over 2100 m asl, a central part formed by hilly landscapes and basin, and a western coastal and southern part largely connected to the more recent evolution of the northern Tyrrhenian Sea (Fig. 3). The geological evolution of Tuscany is related to the Northern Apennines fold-thrust belt formed during the Tertiary due the collision between the African plate to the European plate. After the end of the collision stage, during the Mio-Pliocene the tectonic regime changed from compressional to extensional characterized by low- and high-angle normal faults leading to vertical uplift and exhumation coupled with several eustatic transgressive-regressive cycles with the formation of basins characterized by marine and continental deposition. At the end of Pliocene and during the Quaternary, the Tuscany area underwent to stronger vertical uplift movements that brought to the definitive emersion of the area, volcanic activity, and formation of the present-day landscape (see Carmignani et al., 2004, 2013; Coltorti et al., 2017 and references therein). The current morphology reflects the main recent and present-day surface processes responsible for the landscape modelling in terms of erosion and deposition. These processes (i.e. alluvial, slope etc.) lead to the deposition of mostly unconsolidated cover formations with different thicknesses according to the local geomorphological setting. The presence of less consolidated cover formations overlaying more rigid formations are expected to be at the origin of important seismic amplification phenomena (Pieruccini et al., 2022).

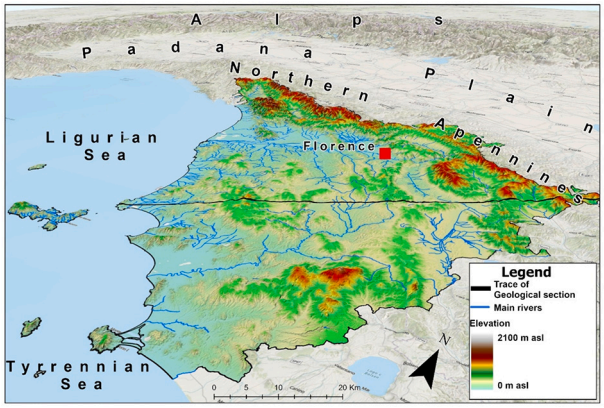

Fig. 3. View of the Tuscany landscape from South. The complex tectono-stratigraphic evolution of Tuscany region is reflected on its geomorphological setting that is characterized by NNW–SSE trending morphological highs (mountain ridges), alternating with wide morphological lows (basins and valleys) (Coltorti and Pieruccini, 1997; Coltorti et al., 2017). The black line is the trace of the representative section reported in Fig. 5.

According to the available extensive geological dataset (Banche dati cartografia geologica, n.d., Regione Toscana, https://www.regione.toscana.it/-/banche-dati-cartografia-geologica) and the available literature (Carmignani et al., 2013 and reference therein) in Tuscany outcropping metamorphic, sedimentary, and magmatic rocks can be grouped into a number of major MSDs (Table 3) belonging to the coverage or to bedrock units each characterized by a peculiar stratigraphical position and lithological characteristics.

The outcome of this analysis results in about 80,000 outcrops each bearing the information reported in Table 3, which provide an overview of the distribution over a large area of the different MSDs and of their reciprocal stratigraphical settings (Figs. 4 and 5). The map of MSDs and the included section show the geographical distribution of the outcropping terrains across the Region (Fig. 4 and Fig. 5).

As a second step, Logs relative to each outcrop in Fig. 4 are defined as a succession of layers each characterized by a thickness range and dominant lithotype. It is worth to note that in this study, differently from (Pieruccini et al., 2022), the MSD classification plays a major role since it constrains the succession of overlapping formations, from the lowermost units of the bedrock (MSD 80 in Table 3) to the uppermost units of the cover terrains (MSDs 11, 12 in Table 3). Considering the overall

Table 3
The Geological-Geomorphological model of the Tuscany Region including the classification of its morpho stratigraphic MSDs (MSD) based on their stratigraphical and geomorphological positions. Notably, MSDs 11 and 12 are not arranged in stratigraphic since they are stratigraphically 'lateral', i.e., they represent alternative outcrop. The provided information encompasses the primary geological characteristics of each MSD, the total thickness ranges, the lithotype, its potential stratigraphic sequence, and the corresponding thicknesses.

MSD	Bedrock-Cover Terrains	Geomorphological position	Outcrop description and age	Lithotypes	Thickness range for lithotypes
11	Cover	Valleys and slopes	Gravelly, sandy and clayey alluvial, slope, coastal and glacial deposits (Quaternary)	G, S, C	50–100
12			Gravelly, sandy and clayey alluvial, slope, coastal and glacial deposits (Quaternary)	G, S, C	<50
20		Slopes	Volcanics, pyroclastics and lavas (Quaternary)	L, S, V, W	10–100
30		Basins	Continental sandstones, conglomerates and clays of the tectonic basins (Early-Middle Pliocene)	V W	3–150 3–50
41		Basins	Marine, coastal and continental sandstones, conglomerates and clays of the tectonic basins (Early-Middle Pliocene)	V W	3–300 3–300
42		Basins	Marine, coastal and continental sandstones, conglomerates and clays of the tectonic basins (Late Messinian)	V W	3–50 3–100
43		Basins	Marine, coastal and continental sandstones, conglomerates and clays of the tectonic basins (Messinian)	V W	3–50 3–100
44		Basins	Marine, coastal and continental sandstones, conglomerates and clays of the tectonic basins (Middle Miocene)	V W	3–50 3–100
45	Bedrock	Basins	Clayey lacustrine deposits of the tectonic basins (Early-Middle Miocene)	W	3–50
50		Ridges	Deep sea mainly mixed limestones and claystones of the Ligurian, Subligurian and Epiligurian Units (Creataceous-Early Miocene)	L V W	3–300 3–150 3–150
60		Ridges	Foreland arenaceous dominated successions of the Tuscan Units (Oligocene-Miocene)	V W	3–300 3–300
70		Ridges	Limestone dominated successions of the Tuscan Units (Triassic-Eocene)	L V W	3–300 3–300 3–300
80		Ridges	Metamorphic complex of the Tuscan Units and Paleozoic Basement (Paleozoic to Eocene)	L, V, W	300

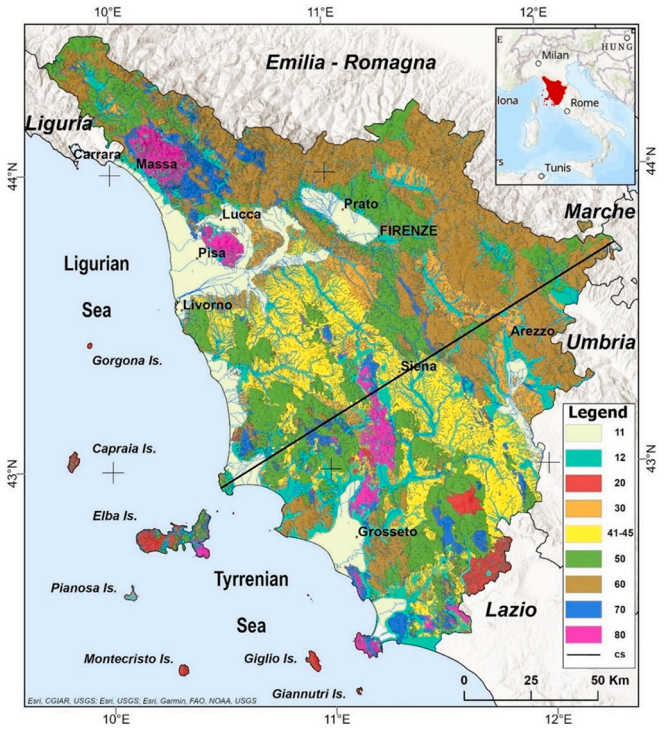

Fig. 4. Map of the outcrops relative to the morpho stratigraphic domains (MSDs) of the Tuscany region. The Legend shows the MSDs in Table 3, The black line is the trace of the representative section reported in Fig. 5.

morpho-structural setting of the Region (Fig. 5) it is possible to establish the possible Logs for any outcrop approximated to the depth of 300 m, considered of interest for seismostratigraphic modelling (Fig. 7). By considering the ordering of MSDs, one can develop a matrix (Fig. 7) considering all the theoretical overlap relationship from the higher units (MSD 11) to the lower ones (MSD 80). As shown in the matrix of Fig. 6, the number of possible logs increases upward in the stratigraphical order for bedrock, while the terrain of the shallower cover terrains (MSD 11,12, 20) overlies unconformably all older MSDs. The highest number of Logs are recorded for the MSD 41–45 and 30 corresponding to the most settled areas of the Region.

As a whole, 4230 typologies of outcrops have been finally identified, each with a specific stratigraphic configuration and distributed throughout the whole study areay. Approximately 63 % of the generated outcrops are characterized by outcropping sedimentary covers (MSD 11 and MSD 12), while the remaining portion consists of stratigraphic sequences where geological bedrock outcrops (Fig. 7).

Seismic response relative to each outcrop has been modeled by considering as input the respective response spectrum as deduced by the Italian Seismic Hazard Map (*https://esse1-gis.mi.ingv.it/*) at reference soil conditions (flat morphology and outcropping rigid rock with Vs > 800 m/s). Hundred random stratigraphical sequences constrained by available information have been considered for each outcrop. This allows exploring expected range of amplification factors, considering the propagation of uncertainty relative to each local seismostratigraphical condition for the considered lithological unit.

About 2 10^6 simulations of the local 1D seismic response have been performed. Despite of the fact that stochastic Vs profiles were developed down to a depth of 300 m, in less than 10 % of cases the depth of the engineering bedrock (where the input motion is applied) was deeper than 100 m and less than 1 % deeper than 150 m. Since the parameterization of Vs profiles is adequately supported by available data to a depth of 100 m (Falcone et al., 2021; Romagnoli et al., 2022) this implies that the role of the extrapolated Vs values generally played a minor role on the outcomes.

4. AF estimates relative to the outcrops in the Tuscany region

The distribution of median of AF values relative to the considered

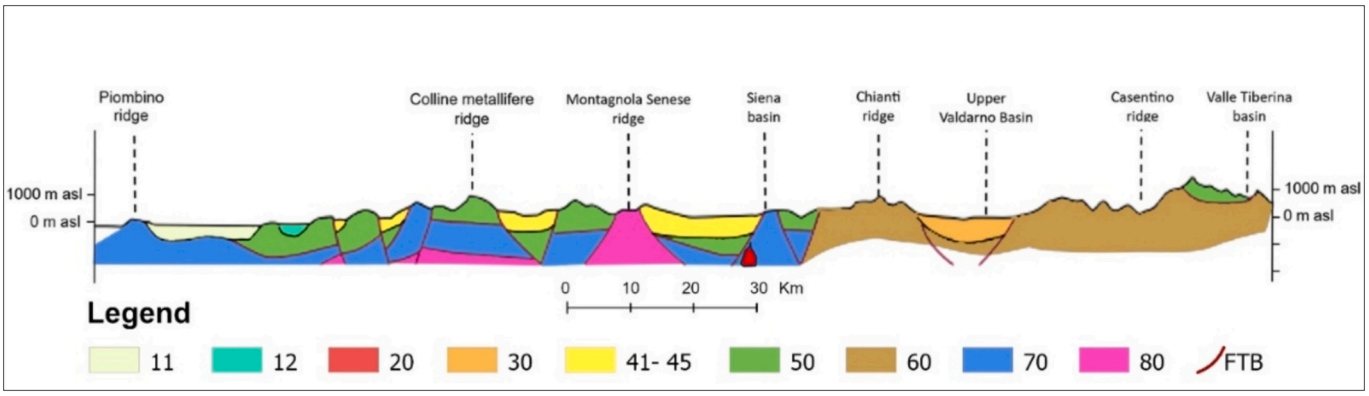

Fig. 5. Representative Geological-Geomorphological section of the Tuscany evidencing the surface and subsoil setting of morpho stratigraphic MSDs represented in Fig. 4. The representation of cover terrains is underestimated due to problem of scale. Numbers and colours in the boxes are related to those in and legend of Fig. 4. The data relative to subsurface settings are modified from geological section published by Carmignani et al. (2013).

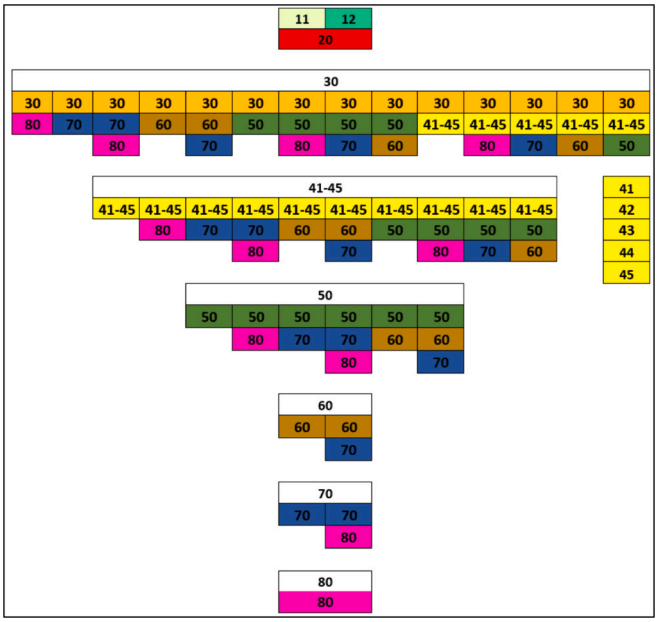

Fig. 6. Matrix for evaluating the possible overlapping order and combinations of the outcrops relative to each MSD. Numbers and colours in the boxes are related to those in and legend of Fig. 4.

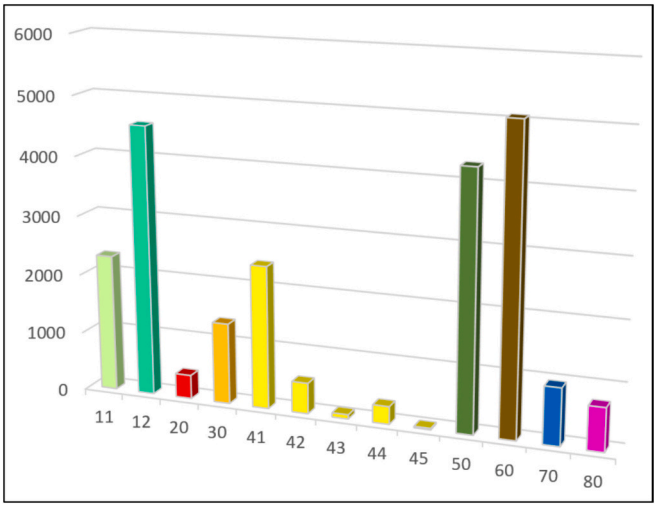

Fig. 7. Areal coverage of outcrops in the Tuscany region as a function of the respective MSD. On the vertical axis the area covered by each MSD is expressed in km^2. Colours correspond to those in and legend of Fig. 4.

outcropping MSDs is presented in the form of a box-plot diagram of Fig. 8. The three boxes for each MSD represent the distributions of values obtained relative to the three ranges of periods considered (0.1–0.5 s, 0.4–0.8 s, 0.7–1.1 s respectively). The plot in Fig. 8, puts in evidence that significantly different AF values have been obtained for the considered MSDs. This outcome is far from being obvious, due to the large variability ranges attributed to the MSDs relative to each outcrop. This outcome is of primary importance, since demonstrates that the geological data provided by the detailed geological maps at regional scale may be very informative about the expected seismic response at the considered sites in the lack of more detailed investigations. However, important trends can be observed in the distribution of AFs values for the different MSDs. The CTs show notable differences between MSD 11 (the thicker alluvial deposits of the major floodplains), MSD 12 (the shallower alluvial and slope deposits), and MSD 20 (the Quaternary volcanics).

Amplification effects reduce with increasing the vibration period considered, except in the case of the MSD 11, which is representative of the thick cover terrains of the major alluvial plains. In this case, as expected, de-amplification effects are revealed at smaller vibration periods, with a median AF value below 1. The de-amplification effects in the short period range when thick sedimentary basins exist have been experimentally documented in the case of the Kik-Net network (Paolucci et al., 2021).

The higher AF values of MSD 12 and their distribution suggest the importance of the thickness of Coverage terrains scattered along the slopes and minor floodplains of the landscape. MSD 20 presents lower AF values perhaps in relation to the presence of thick massive lava flows. A similar notable range of AF values can be observed for Mio-Pliocene continental and marine deposits of tectonic basins, consisting mostly of thick clayey, sandy, and conglomeratic facies. Only MSD 45 shows higher amplification factors, although these are shallow Miocene lacustrine clay deposits occurring in only 21 km^2. Other important trends can be observed for MSDs 50 and 60 whose AF values are higher than MSD 70 and 80 probably due to greater lithological heterogeneity.

More surprising could be considered the large amplifications where the geological bedrock outcrops. However, one must consider Vs data relative to these formations (Romagnoli et al., 2022) indicate the general presence of weathering and alteration processes where these relatively old formations outcrop. This is responsible for a rapid increase of rigidity in the shallowest part of the velocity profile, which generates sharp shallow seismic impedance contrasts responsible for energy trapping

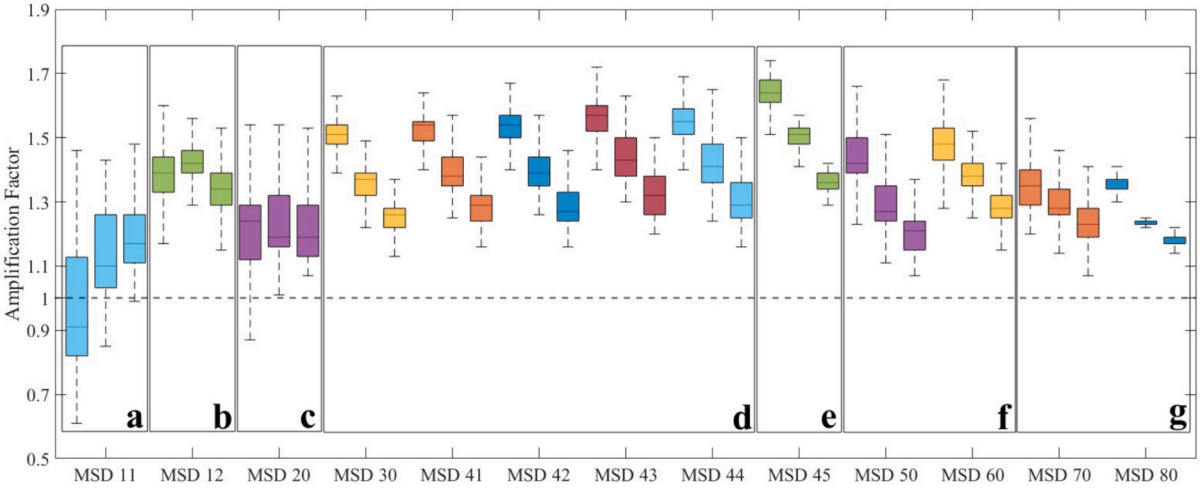

Fig. 8. Bow-Whiskers plots relative to the distribution of median amplification factors for approximately 80,000 outcrops analyzed in the Tuscany region is depicted. Different colours discretize the various MSDs in Fig. 4. The three colored boxes for each MSD represent the distributions of amplification factors across three ranges of period [0.1–0.5 s], [04–0.8 s], [0.7–1.1 s]. Boxes labeled from (a) to (g) highlight the groups MSDs characterized by a similar distribution of amplification factors.

and resonance of upgoing seismic waves and, ultimately, of amplification effects. This suggests that the assumption of a potential correspondence between engineering and geological bedrock is generally unreliable.

A major factor responsible for variations in the estimated AF is the estimated depth of the engineering bedrock. Most of MSDs exhibit a weak linear correlation between amplification factors and depths of the engineering bedrock. This correlation tends to be negative when accounting for deep sedimentary covers (MSD 11), owing to the greater variability in engineering bedrock depth (30-150 m). This trend is also evident in other MSDs, although less pronounced due to a narrower range of the relative depths of the engineering bedrock. Specifically, units characterized by shallow sedimentary covers or composed only of geological bedrock typically exhibit a engineering bedrock confined to depths ranging from 20 to 50 m. In some cases, AF within this depth range also demonstrate a positive linear correlation. As expected, within each MSD a significant correlation is also found between median AFs and the harmonic average of the Vs values above the engineering bedrock. This relation, which is found to be almost always slightly negative, has been recognized in all the range of periods and for all the MSDs analyzed. The only unit that deviates from this trend is unit MSD 11, where a distinct positive correlation between AF and the harmonic average of Vs values to the engineering bedrock is observed.

As an effect of nonlinearity of soil behaviour, experimental data (e.g.., Regnier et al., 2016) suggest that increasing load implies a relative reduction of amplification effects in the range of short periods and an increase in the long period range. The period marking the transition between the two MSDs is site dependent and inversely correlates with the site fundamental resonance frequency: the lower is the frequency the larger is the 'transition period' separating increasing and decreasing amplification effects. In the present context, a negative correlation is thus expected between the PGA at the reference subsoil (as a proxy for the entity of input seismic load) and AF in the first range of periods; a positive correlation is instead expected relative to AF values in the long period range. Table 4 illustrates the Pearson correlation coefficient between the reference peak ground acceleration and the median AFs. As expected, due to non-linear soil behaviour, a negative correlation was observed at short periods, while AF values at longer periods exhibit a positive correlation. The only significant exception concerns MSD 11, i.e., in correspondence of deep sedimentary cover. Possibly this is the effect of the larger depth of the engineering bedrock which may result in longer resonance periods and the consequent displacement of the transition period below 1 s. An alternative hypothesis is that this behaviour may be related to the presence of inversions in Vs profiles that could mask the influence of soil nonlinearity and could be responsible of a relative reduction of amplification effects in the three ranges of period.

However, focusing on median values may be misleading since median AF values may represent an under conservative estimate of the actual amplification effect since the variability of simulation outcomes is not accounted for. A more conservative approach could be considering any upper percentile of the relevant distribution of values (e.g., Peruzzi et al., 2016; Andreotti et al., 2018). In this view, the geographical distribution of AF values corresponding to 84th percentile of the respective distribution is reported relative to the range of periods 0.1/0.5 s (Fig. 9). As one can see, geological heterogeneities reflect on the AF values.

5. Testing AF values relative to the Tuscany region

To assess the reliability of outcomes of the analysis here performed, relative AF values were compared with outcomes of detailed Seismic Microzonation studies performed out by following the Italian standards (SM Working Group, 2015) in the Tuscany area. These studies have been carried out thanks to the Italian Seismic Microzonation multiannual program starting in 2010, financed by the Italian Civil Protection Department to involve local authorities in Italy, such as single municipalities, in seismic defense, city planning, and land use rules (Albarello, 2017; Paolucci et al., 2020). The second and third levels of seismic microzonation studies were retrieved from the national database of Seismic Microzonation (Commissione Tecnica MS, 2018) and were considered in the comparative analysis. It is worth to note that areas

Table 4
Pearson correlation coefficient between reference Peak Ground Acceleration from the national hazard model and estimated amplification factor for all MSDs in the three ranges of period.

MSD	11	12	20	30	41	42	43	44	45	50	60	70	80
[0.1–0.5 s]	−0.48	−0.45	−0.63	−0.22	−0.45	−0.17	−0.33	−0.27	−0.50	−0.31	−0.62	−0.31	−0.42
[0.4–0.8 s]	−0.43	0.00	−0.27	0.39	−0.11	0.33	0.04	0.12	0.10	0.12	0.36	0.19	−0.12
[0.7–1.1 s]	−0.32	0.30	−0.07	0.49	−0.03	0.39	0.12	0.19	0.37	0.26	0.56	0.31	0.26

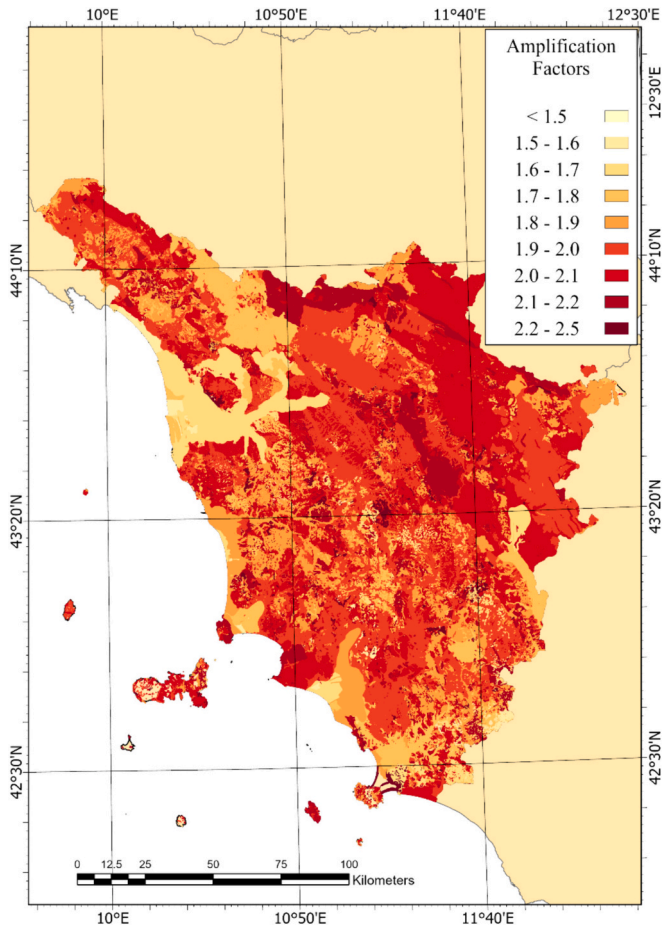

Fig. 9. 84th percentile of the distribution of AF values relative to the period range 0.1–0.5 s.

considered in these studies concern urbanized areas and that these only represent less than 2 % of the whole study area. Anyway, approximately 1500 benchmark areas where seismic microzonation studies were performed: at these sites outcoming AF values (AF_{SM}) have been compared with those determined in the present study. This comparison must account for uncertainty affecting our estimates and thus the eventual biasedness of these last onese can only be tested in a probabilistic sense. To this purpose, we assume that the set of *AF* values determined by numerical simulations at each site represent the population of the values compatible with the adopted constraints. The probability distribution representative of this population is assumed to be Log-Normal. This implies that the distribution of ln*(AF)* values is a Gaussian with parameters μ and σ both estimated from the outcomes of the numerical simulations. In this view, the *AF* value O_i provided by the local microzonation study at any *i-th* site can be seen as the realization of a stochastic process characterized by the probability distribution assessed by numerical simulations for that site. In this hypothesis (H0 in the statistical jargon), the stochastic variate

$$Z_i = \frac{\mu_i - ln(O_i)}{\sigma_i} \tag{2}$$

follows the standardized Gauss distribution. If one considers n sites where one of the MSDs in Table 3 outcrops, the random variate

$$\chi^2_n = \sum_{i=1}^{n} Z_i^2 \tag{3}$$

is expected to follow the chi-square distribution with n degrees of freedom. This allows checking the eventual biasedness of the estimates provided in this study for the outcrop of concern by considering the exceedance probability associated to the χ^2_n determined for the considered outcrop. By adopting a relatively low significance level (0.1) is considered, a threshold value for χ^2_n can be determined: if the experimental value is below the threshold, the hypothesis H0 cannot be rejected on a statistical basis and the estimates provided by numerical simulations can be considered unbiased. In Table 5, the χ^2_n values relative to the outcropping MSDs are reported for each range of periods, along with the respective threshold values.

As one can see, all the outcrops have been considered, except the 45 and 80 ones, where no microzonation study has been performed. One can see that only in the case of the MSD 70, the hypothesis H0 can be rejected relative to the first range of periods: in all the other cases the unbiasedness of the estimates provided by numerical simulations is confirmed.

6. Conclusion

A new approach has been here proposed to provide an extensive evaluation of 1D seismic amplification effects induced by the local seismostratigraphical configuration. This approach is based on combination of regional scale morphostratigraphic data from geological maps and extensive numerical simulations. The procedure here proposed aims at exploiting the large amount of geological information provided by detailed geological maps to exhaustively cover the study area. The stochastic numerical simulations carried out by considering geological constraints allow estimating expected amplification effects along with the respective uncertainty margins by accounting for uncertainty affecting input data. Thus, feasibility of the proposed approach has been tested in the Tuscany area in central Italy, where complex and highly variable geological configurations exist. The statistical comparison of detailed seismic microzonation studies carried out in the area by following Italian standards allowed to check the general unbiasedness of results provided by the proposed approach.

The probabilistic formulation of the outcomes will allow to combine outcomes of different approaches to the large scale estimate of seismic amplification phenomena. As an example, outcomes of the present study and those by Falcone et al., 2021 should be seen as complementary and not alternative since they are considering different input information (geological and morphological respectively): if jointly considered (e.g., in the frame of Bayesian view) they could provide better constrained large-scale estimates. Moreover, to overcome the possible limitations relative to the 1D approach considered in both the methodologies, local topographic configurations assessed at the same regional scale (e.g., Fantozzi et al., 2023) could be also implemented by following the

Table 5
Values of the χ^2_n values (eq.[2]) relative to the outcropping MSDs (see Table 3). n is the number of sites considered for the relevant outcropping MSD, which corresponds to the degrees-of-freedom of the representative chi-square distribution (see text for details).

		χ2			Significance Threshold
MSD	n	0.1–0.5 s	0.4–0.8 s	0.7–1.1	$p < 0.1$
11	45	15	18	21	58
12	665	182	250	439	712
20	125	169	136	250	146
30	146	74	99	201	168
41	87	44	27	82	104
42	7	0	3	3	12
43	16	14	9	5	24
44	2	4	2	2	5
45	0	–	–	–	–
50	116	119	105	90	136
60	276	191	159	189	307
70	4	**10**	6	4	8
80	0	–	–	–	–
Global	1489	823	814	1286	1559

approach of the current seismic rules (e.g. CEN, 2004).

Anyway, the procedure here proposed presents important limitations preventing the application of its outcomes for the design of single structures. The use of statistically based parametrizations, the restrictive assumptions relative to the possible geometrical relationships between conterminous outcrops, the assumption of a single prevalent lithology relative to any considered outcrops, etc., makes the proposed estimates of the 1D amplification effects valid in a statistical sense only: by no way these should be considered as alternative to detailed seismostratigraphical and geotechnical characterizations. Anyway, these outcomes could be of great importance for the preliminary identification of potentially critical situations where detailed microzonation studies are not available. This may also represent a valuable input of the risk assessment at regional scale or where distributed facilities or vulnerable assets exist.

CRediT authorship contribution statement

P. Pieruccini: Writing – review & editing, Writing – original draft, Methodology, Conceptualization. **P.L. Fantozzi:** Writing – review & editing, Writing – original draft, Methodology, Data curation, Conceptualization. **N. Carfagna:** Writing – review & editing, Software, Data curation. **I. Gaudiosi:** Writing – review & editing, Data curation. **D. Albarello:** Writing – review & editing, Writing – original draft, Supervision, Project administration, Methodology, Funding acquisition, Formal analysis, Conceptualization.

Declaration of competing interest

The authors declare that they have no known competing financial interests or personal relationships that could have appeared to influence the work reported in this paper.

Data availability

Data will be made available on request.

Acknowledgements

Many thanks are due to the Editor and to the four anonymous referees for their fruitful critical comments and suggestions. The present study has been developed in the frame of the PRIN project “Mapping SEismic site effects at REgional and NAtional scale - SERENA” (2020MMCPER) financially supported by the Italian Ministry of University and Research (MUR).

Appendix A

The macrogroup concept proposed by Romagnoli et al. (2022) was specifically employed to categorise and group together soil and rock samples that exhibited comparable mechanical features. The authors have categorised the materials into different lithotypes based on the statistical comparison between intra and inter group variability of experimental Vs value relative to each lithotype. The lithotype “G” represents gravels, specifically GW, GP, GM, GC, and RI engineering geological groups. The lithotype “S” represents sands and silts, including SW, SP, SM, SC, MH, and ML engineering geological group. The lithotype “C” represents clays, such as CL, CH, OL, OH, and PT engineering geological group. The lithotype “L” represents LP, LPS, SFLP, SFLPS, and LC engineering geological group. The lithotype “V” represents GR, GRS, ALS, AL, SFALS, and CO engineering geological group. Lastly, the lithotype “W” represents COS and weathered and/or fractured SFGR, SFGRS, SFAL, SFCO engineering geological group. The parametrization of the layers to be modeled was also based on a previous study: the dataset provided by Gaudiosi et al. (2023). The authors integrated the complete collection of geotechnical data obtained from seismic microzonation studies conducted in Italy and established a repository in which each curve was linked to the corresponding engineering geological units examined in the seismic microzonation research. However, to ensure consistency with the lithotypes defined in the prior study of Romagnoli et al. (2022), the curves used for the simulations in this study were recalculated and utilised for the purpose of the dynamic parametrization. These curves were obtained by computing the new parameters for the laws that describe the non-linear soil behaviour of the two cover units: “S” and “C”.

It has to be underlined that the dataset examined by Gaudiosi et al. (2023) demonstrates a lack of knowledge for the deepest layers: the depth of investigation of the dataset is limited to about 40 m (and to a mean confining effective pressure $\sigma' > 180–200$ kPa). To overcome this problem, a depth-dependent model from the soil behaviour established in Eastern North America (denoted as EPRI, 1993) was used to retrieving the G/G_0 and D values. The average G/G_0 and D curves of the EPRI model are available in the depth range of 0–305 m (Fig. 1a, b, c and d). In this study, the variability of the G/G_0 and D curves for “S” and “C” in the depth range 0–40 m, 40–150 m and 150–300 m was compared with the ones denoted as EPRI. As depicted in Fig. A1, the G/G_0 and D curves for S and C and their relative range of ± sigma were observed to lie within the EPRI curve, while considering a depth interval ranging from 15 to 150 m for “C” and from 0 to 86 m for “S”. Beyond this range, EPRI curves for 500–1000 ft (152–305 m) were adopted in this study.

For “G”, we adopted the results obtained from Rollins et al. (1998) (average interval), for the depth interval ranging from 0 to 150 m, and Rollins et al. (2020), for the depth interval ranging from 150 to 300 m. Darendeli (2001) was used for describing the variability in this case. The use of a source of literature is due to the characteristics of the archive used for the parametrization for “S” and “C”: specimens for coarse soils contain finer levels, which may induce misinterpretations of the non-linear soil behaviour for gravels. Thus, in the latter case, the chosen G/G_0 and D curves are those provided by the correlation given for a uniformity coefficient (Cu) of 10, and a confining pressure value of 600 kPa. As shown in Fig. A1e and A1f, the G/G_0 and D curves for “G” becomes more linear (shifted to the right) as the depth (and thus the confining pressure) increased. For a given confining pressure, the G/G_0 curve for gravel results offset slightly to the left of the corresponding curve for “S” defined in this study. For similar conditions, the D curves for G do not show the same shifting than those for “S”: the trend is inverted. This likely reflects the potential variations in the soil behaviour, which may be due to higher fines contents or soil plasticity captured by the seismic microzonation dataset (blue curve in Fig. A1f extracted by the archive published in Gaudiosi et al. (2023). The initial archive also exhibits a deficiency in laboratory analyses conducted on geological bedrock units with the fewest available samples. In this study, a fixed averaged damping value was employed for range of depth [0–20 m); [20 - 100 m); [100 m - ∞), which was determined using a commonly used heuristic formula: D_0 (%) = [10/(2*Vs)]*100 (Parolai et al., 2022). Darendeli (2001) was used for describing the variability in these cases. Specifically, all the G/G_0 and D curves presented in Table A1 were used.

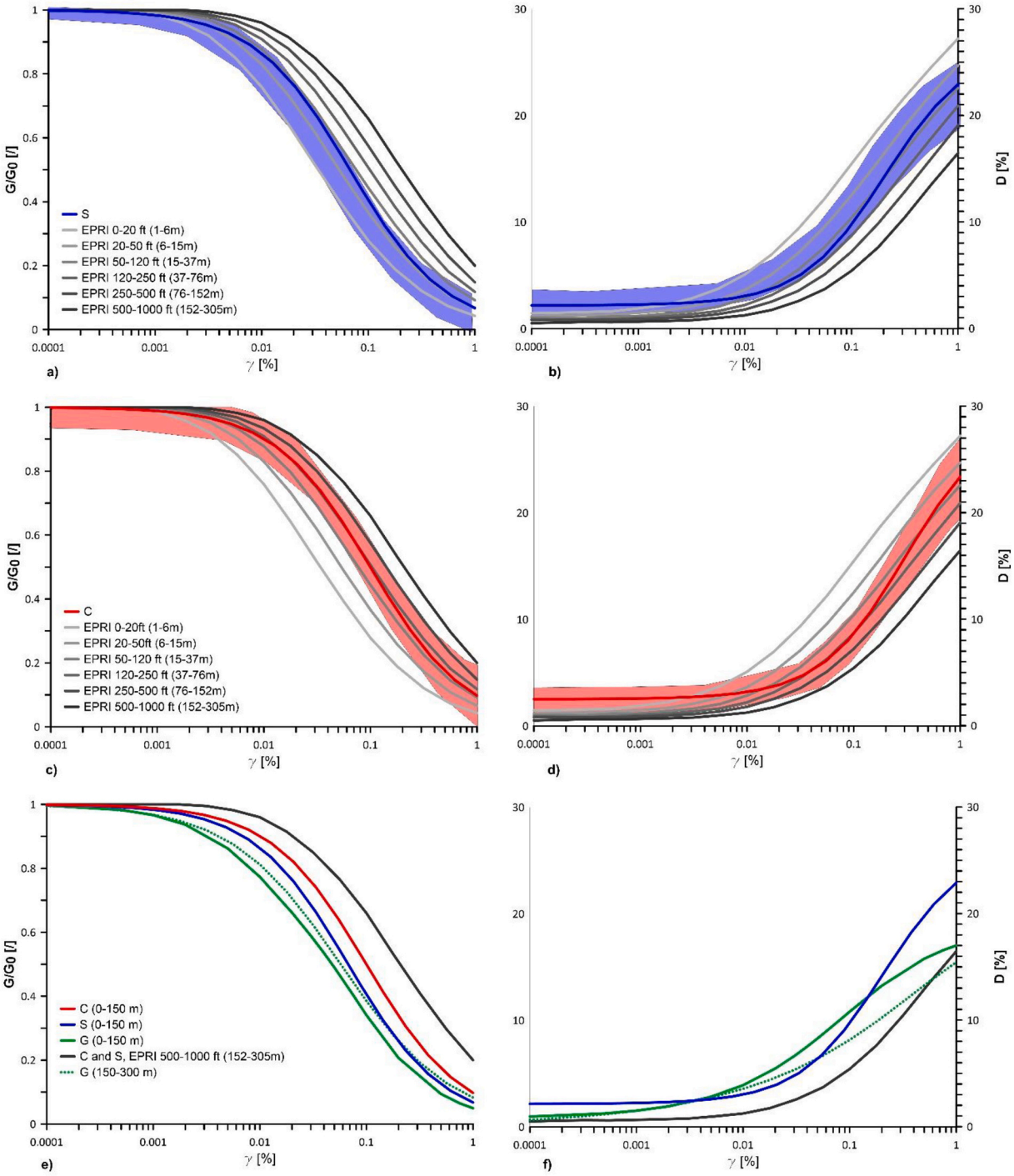

Fig. A1. G/G0 and D curves used in this study. a) and b), c) and b) subplots refer to sands "S" and clays "C" compared with EPRI curves, respectively. e) and f) subplots refer to the sands, clays and gravels non-linear behaviours used in this study and analyzed with respect to the confining pressure values increasing.

Table A1
Parameters used in this study to describe the mechanical and dynamic behaviour of the relevant lithotype variability as a function of depth H (in m). For each lithotype the following information is reported: unit weight (and relative reference), median Vs as function of depth, standard deviation of the Vs values in natural logarithms, reference relative to G/G0 and damping curves (1–3: this study, modified after Gaudiosi et al., 2023; 2: EPRI 93 (500-1000 ft); 4: Rollins et al., 1998; 5: Rollins et al., 2020), G/G0 and damping curves; inter-layer correlation between Vs values in subsequent layers (see, range of depths for the considered parametrization. Unit weights were computed from Gaudiosi et al. (2023).

Lithotype	Unit weight (kN/m^3)	Vs (H)	σ_{logVs}	G/G_0 and D curves	Standard deviations of G/G0 and D curves	Inter-layer correlation	Depth range
C	19.4	189*H^0.187	0.441	1	0.09764*exp.(−0.4429*G) - 0.07291 *exp.(−75.58*G); 2.416*exp.(0.02*D) -1.819*exp.(−0.1347*D)	1–0.131*exp.(−0.069*H + 0.277)	0-28 m
				1	0.09764*exp.(−0.4429*G) - 0.07291*exp.(−75.58*G); 2.416*exp.(0.02*D) -1.819*exp.(−0.1347*D)	0.976	28-150 m
				2	Darendeli, 2001		150-300 m
S	19.3	190*H^0.267	0.436	3	−1.17*exp.(2.247*G) + 1.23*exp.(2.199*G); 2.361*exp.(0.0209*D) -1.788*exp.(−0.1425*D)	1–0.131*exp.(−0.069*H + 0.277)	0-28 m
				3	−1.17*exp.(2.247*G) + 1.23*exp.(2.199*G); 2.361*exp.(0.0209*D) -1.788*exp.(−0.1425*D);	0.976	28-150 m
				2	Darendeli, 2001		150-300 m
G	19.8	217*H^0.301	0.433	4	Darendeli, 2001	1–0.131*exp.(−0.069*H + 0.277)	0-28 m
					Darendeli, 2001	0.976	28–150 m
				5	Darendeli, 2001	0.976	150–300 m
L	20.5	257*H^0.398	0.477	D0 = cost (1 %)	Darendeli, 2001	1–0.211*exp.(−0.130*H + 0.311)	0-20 m
				D0 = cost (0.5 %)	Darendeli, 2001	0.98	20-100 m
				D0 = cost (0.3 %)	Darendeli, 2001	0.98	100–300 m
V	21.1	183*H^0.407	0.411	D0 = cost (1 %)		1–0.211*exp.(−0.130*H + 0.311)	0–20 m
				D0 = cost (0.5 %)	Darendeli, 2001	0.98	20-100 m
				D0 = cost (0.3 %)		0.98	100-300 m
W	21.0	170*H^0.358	0.410	D0 = cost (1 %)	Darendeli, 2001	1–0.211*exp.(−0.130*H + 0.311)	0-20 m
				D0 = cost (0.5 %)	Darendeli, 2001	0.98	20-100 m
				D0 = cost (0.3 %)	Darendeli, 2001	0.98	100-300 m

References

Acunzo, G., Falcone, G., di Lernia, A., Mori, F., Mendicelli, A., Naso, G., Albarello, D., Moscatelli, M., 2024. NC92Soil: a computer code for deterministic and stochastic 1D equivalent linear seismic site response analyses. Comput. Geotech. 165, 105857 https://doi.org/10.1016/j.compgeo.2023.105857.

Albarello, D., 2017. Extensive application of seismic microzoning: methodological and socio-political issues in the Italian experience. Boll. Geofis. Teor. 58 (4), 253–264. https://doi.org/10.4430/bgta0205.

Allen, T.I., Wald, D.J., 2009. On the use of high-resolution topographic data as a proxy for seismic site conditions (VS30). Bull. Seismol. Soc. Am. https://doi.org/10.1785/0120080255.

Andreotti, G., Famà, A., Lai, C.G., 2018. Hazard-dependent soil factors for site-specific elastic acceleration response spectra of Italian and European seismic building codes. Bull.Earthq.Engg. 16, 5769–5800. https://doi.org/10.1007/s10518-018-0422-9.

Banche dati cartografia geologica, Regione Toscana. (n.d.). https://www.Regione.Toscana.It/-/Banche-Dati-Cartografia-Geologica.

Carmignani, L., Lazzarotto, A., Brogi, A., Conti, P., Cornamusini, G., 2004. Carta Geologica della Toscana - Geological map of Tuscany, 1:250.000 scale. 32nd International Geological Congress - Italia, 20-28 August, Florence.

Carmignani, L., Conti, P., Cornamusini, G., Pirro, A., 2013. Geological map of Tuscany (Italy). J. Maps 9 (4), 487–497. https://doi.org/10.1080/17445647.2013.820154.

CEN (Comité Européen de Normalisaton), 2004. EN 1998-1. Eurocode 8: Design of structures for earthquake resistance - Part 1: General rules, seismic actions and rules for buildings, European Committee for Standardization. Brussels, Belgium.

Cesarano, M., Porchia, A., Romagnoli, G., Peronace, E., Mendicelli, A., Nocentini, M., Naso, G., Castenetto, S., Catalano, S., Moscatelli, M., 2022. Multiscale geothematic maps for using the database from the Italian Seismic Microzonation Project: an example of application in the Calabria Region (Southern Italy). Ital. J. Geosci. 141 (1), 35–52. https://doi.org/10.3301/IJG.2022.03.

Coltorti, M., Pieruccini, P., 1997. Middle-Upper Pliocene 'compression' and middle Pleistocene 'extension' in the East-Tiber Basin (Central Italy): from 'perched' to 'extensional' basin in the Northern Apennines. Il Quaternario 10 (2), 521–528.

Coltorti, M., Fantozzi, P.L., Pieruccini, P., 2017. Tuscany Hills and Valleys: Uplift, Exhumation, Valley Downcutting and Relict Landforms, pp. 245–255. https://doi.org/10.1007/978-3-319-26194-2_21.

Commissione Tecnica MS, 2018. Standard di rappresentazione e archiviazione informatica degli Studi di MS vers.4.1.

Darendeli, M.B., 2001. Development of a New Family of Normalized Modulus Reduction and Material Damping Curves.

Di Capua, G., Peppoloni, S., Amanti, M., Cipolloni, C., Conte, G., 2016. Site Classification Map of Italy Based on Surface Geology. Geol. Soc. Eng. Geol. Spec. Publhttps://doi.org/10.1144/EGSP27.13.

EPRI, 1993. Guidelines for Determining Design Basis Ground Motions. EPRI: Final Report. Electric Power Research Institute, EPRI.

Falcone, G., Acunzo, G., Mendicelli, A., Mori, F., Naso, G., Peronace, E., Porchia, A., Romagnoli, G., Tarquini, E., Moscatelli, M., 2021. Seismic amplification maps of Italy based on site-specific microzonation dataset and one-dimensional numerical approach. Eng. Geol. 289, 106170 https://doi.org/10.1016/j.enggeo.2021.106170.

Fantozzi, P.L., Paolucci, E., Pieruccini, P., Albarello, D., 2023. Automatic identification of sites prone to topographic seismic amplification effects by the current seismic codes. Soil Dyn. Earthq. Eng. 174, 108212 https://doi.org/10.1016/j.soildyn.2023.108212.

Forte, G., Chioccarelli, E., De Falco, M., Cito, P., Santo, A., Iervolino, I., 2019. Seismic soil classification of Italy based on surface geology and shear-wave velocity measurements. Soil Dyn. Earthq. Eng. https://doi.org/10.1016/j.soildyn.2019.04.002.

Gaudiosi, I., Romagnoli, G., Albarello, D., Fortunato, C., Imprescia, P., Stigliano, F., Moscatelli, M., 2023. Shear modulus reduction and damping ratios curves joined with engineering geological units in Italy. Sci. Data 10 (1), 625. https://doi.org/10.1038/s41597-023-02412-8.

Jin, X., Li, X., Huang, Y., 2024. DEM analysis on diffuse failure of soil slope triggered by earthquakes. Eng.Geol. 339, 107640 https://doi.org/10.1016/j.enggeo.2024.107640.
Kramer, S.L., 1996. Geotechnical Earthquake Engineering. Prentice-Hall, New Jersey, p. 653.
Kwok, O.L.A., Stewart, J.P., Kwak, D.Y., Sun, P.-L., 2018. Taiwan-specific model for Vs30 prediction considering between-proxy correlations. Earthquake Spectra 34, 1973–1993.
Mendicelli, A., Falcone, G., Acunzo, G., Mori, F., Naso, G., Peronace, E., Porchia, A., Romagnoli, G., Moscatelli, M., 2022. Italian seismic amplification factors for peak ground acceleration and peak ground velocity. J. Maps 18 (2), 497–507. https://doi.org/10.1080/17445647.2022.2101947.
Mori, F., Mendicelli, A., Moscatelli, M., Romagnoli, G., Peronace, E., Naso, G., 2020a. A new Vs30 map for Italy based on the seismic microzonation dataset. Eng. Geol. 275, 105745 https://doi.org/10.1016/j.enggeo.2020.105745.
Mori, F., Gaudiosi, I., Tarquini, E., Bramerini, F., Castenetto, S., Naso, G., Spina, D., 2020b. HSM: a synthetic damage-constrained seismic hazard parameter. Bull. Earthq. Eng. 18 (12), 5631–5654. https://doi.org/10.1007/s10518-019-00677-2.
Moscatelli, M., Albarello, D., Scarascia, Mugnozza G., Dolce, M., 2020. The Italian approach to seismic microzonation. Bull. Earthq. Eng. 18 (12), 5425–5440. https://doi.org/10.1007/s10518-020-00856-6.
Ojomo, O., Rathje, E.M., Wang, P., Lavrendiatis, G., Zimmaro, P., Asimaki, D., Stewart, J. P., 2024. Regional earthquake-induced landslide assessments for use in seismic risk analyses of distributed gas infrastructure systems. Eng.Geol. 340, 107664 https://doi.org/10.1016/j.enggeo.2024.107664.
Paolucci, E., Tanzini, A., Peruzzi, G., Albarello, D., Tiberi, P., 2020. Empirical testing of a simplified approach for the estimation of 1D litho-stratigraphical amplification factor. Bull. Earthq. Eng. *18* (4), 1285–1301. https://doi.org/10.1007/s10518-019-00772-4.
Paolucci, R., Aimar, M., Ciancimino, A., Dotti, M., Foti, S., Lanzano, G., Mattevi, P., Pacor, F., Vanini, M., 2021. Checking the site categorization criteria and amplification factors of the 2021 draft of Eurocode 8 Part 1–1. Bull.Earthq.Engg. 19, 4199–4234. https://doi.org/10.1007/s10518-021-01118-9.
Parolai, S., Lai, C.G., Dreossi, I., Ktenidou, O.-J., Yong, A., 2022. A review of near-surface QS estimation methods using active and passive sources. J. Seismol. 26 (4), 823–862. https://doi.org/10.1007/s10950-021-10066-5.
Peruzzi, G., Albarello, D., Baglione, M., D'Intinosante, V., Fabbroni, P., Pileggi, D., 2016. Assessing 1D litho-stratigraphical amplification factor for microzoning studies in Italy. Bull. Earthq. Eng. 14 (2), 373–389. https://doi.org/10.1007/s10518-015-9841-z.
Pieruccini, P., Paolucci, E., Fantozzi, P.L., Naldini, D., Albarello, D., 2022. Developing effective subsoil reference model for seismic microzonation studies: Central Italy case studies. Nat. Hazards 112 (1), 451–474. https://doi.org/10.1007/s11069-021-05188-5.
Pontrelli, M., Baise, L., Ebel, J., 2023. Regional-scale site characterization mapping in high impedance environments using soil fundamental resonance (f0): New England, USA. Eng. Geol. 315, 107043 https://doi.org/10.1016/j.enggeo.2023.107043.
Rathje, E.M., Ozbey, M.C., 2006. Site-specific Validation of Random Vibration Theory-based Seismic Site Response Analysis. J. Geotech. Geoenviron. Eng. 132 (7), 911–922. https://doi.org/10.1061/(ASCE)1090-0241(2006)132:7(911).
Regnier, J., Cadet, H., P-y, Bard, 2016. Impact of non-linear soil behavior on site response amplitude. Bull.Seism.Soc.Am. 106 (4), 1710–1719. August 2016. https://doi.org/10.1785/0120150199.
Rollins, K.M., Evans, M.D., Diehl, N.B., III, W. D. D, 1998. Shear modulus and damping relationships for gravels. J. Geotech. Geoenviron. Eng. 124 (5), 396–405. https://doi.org/10.1061/(ASCE)1090-0241(1998)124:5(396).
Rollins, K.M., Singh, M., Roy, J., 2020. Simplified Equations for Shear-Modulus Degradation and Damping of Gravels. J. Geotech. Geoenviron. Eng. 146 (9) https://doi.org/10.1061/(ASCE)GT.1943-5606.0002300.
Romagnoli, G., Tarquini, E., Porchia, A., Catalano, S., Albarello, D., Moscatelli, M., 2022. Constraints for the Vs profiles from engineering-geological qualitative characterization of shallow subsoil in seismic microzonation studies. Soil Dyn. Earthq. Eng. 161 https://doi.org/10.1016/j.soildyn.2022.107347.
Schnabel, P.B., Lysmer, J., Seed, H.B., 1972. SHAKE: A Computer Program for Earthquake Response Analysis of Horizontally Layered Sites. Report No.EERC72-12,. University of California, Berkeley.
SM Working Group, 2015. Guidelines for Seismic Microzonation. In: Conference of Regions and Autonomous Provinces of Italy.
Stucchi, M., Meletti, C., Montaldo, V., Crowley, H., Calvi, G.M., Boschi, E., 2011. Seismic Hazard Assessment (2003–2009) for the Italian Building Code. Bull. Seismol. Soc. Am. 101 (4), 1885–1911. https://doi.org/10.1785/012010013.
Thompson, E.M., Wald, D.J., 2012. Developing Vs30 site-condition maps by combining observations with geologic and topographic constraints. In: Proceedings of the 15th world Conference on Earthquake Engineering, Lisbon, 24–28 September.
Thompson, E.M., Wald, D.J., Worden, C.B., 2014. A Vs30 map for California with geological and topographic constraints. Bull. Seismol. Soc. Am. 104, 2313–2321.
Vilanova, S.P., Narciso, J., Carvalho, J.P., et al., 2018. Developing a geologically based Vs30 site condition model for Portugal: Methodology and assessment of the performance of proxies. Bull. Seismol. Soc. Am. 108, 322–337.
Wald, D.J., Allen, T.I., 2007. Topographic slope as a Proxy for Seismic Site Condition and Amplification. Bull. Seismol. Soc. Am. 97 (5), 1379–1395. https://doi.org/10.1785/0120060267.